Available online at www.sciencedirect.com

ScienceDirect

Journal of Taibah University for Science 10 (2016) 718–733

Journal of Taibah University for Science

www.elsevier.com/locate/jtusci

5-Substituted 1H-tetrazoles as effective corrosion inhibitors for mild steel in 1 M hydrochloric acid

Chandrabhan Verma [a], M.A. Quraishi [a,*], A. Singh [a,b]

[a] *Department of Chemistry, Indian Institute of Technology, Banaras Hindu University, Varanasi 221005, India*

[b] *State Key Laboratory of Oil and Gas Reservoir Geology and Exploitation, Southwest Petroleum University, Chengdu, Sichuan 610500, China*

Received 5 August 2015; received in revised form 3 October 2015; accepted 25 October 2015
Available online 7 November 2015

Abstract

The corrosion inhibition efficiency of (*E*)-3-phenyl-2-(1H-tetrazole-5-yl)acrylonitrile (PTA), (*E*)-3-(4-nitrophenyl)-2-(1H-tetrazole-5-yl)acrylonitrile (NTA), and (*E*)-3-(4-hydroxyphenyl)-2-(1H-tetrazole-5-yl)acrylonitrile (HTA) on mild steel in 1 M HCl was tested using experimental and theoretical methods. The results show that the inhibition efficiency increases with the increasing concentration, and maximum values were obtained at a 40 mg L^{-1} concentration. The inhibition efficiency of the studied inhibitors follows the order HTA (98.69%) > NTA (96.60%) > PTA (93.99%). Polarization studies suggest that the tetrazoles behave as cathodic inhibitors. The adsorption of the tetrazoles on the mild steel surface obeys the Langmuir adsorption isotherm. In the present study, the values of the free energy of adsorption ($-\Delta G^0_{ads}$) vary from 34.92 to 39.71 kJ mol^{-1}. The adsorption of the tetrazoles on the mild steel surface is supported by SEM, EDX and AFM studies. Quantum chemical calculations provide good support to the experimental results.

Keywords: Mild steel; EIS; Acid solution; SEM/EDX/AFM and quantum chemical calculation

1. Introduction

Mild steel is a widely used construction material that is easily corroded and solubilized in acid solution during several industrial processes such as acid pickling, industrial cleaning, acid de-scaling and acidization of oil wells [1]. Synthetic inhibitors are extensively used to protect metals against corrosion because of their easy and economical synthesis, good inhibition efficiency, and low cost [2–4]. Previously, it has been reported that most of the efficient inhibitors are synthetic compounds containing heteroatoms (such as N, O, S, and P) in addition to multiple bonds (double and triple bonds) and all forms of aromatic rings [5]. These synthetic inhibitors adhere on the metal surfaces and form a protecting surface film at the metal/electrolyte interfaces. The adsorption of the synthetic inhibitors on the metal surface depends upon numerous factors including the nature and number of potential adsorption sites along with the nature of the metal and testing medium [6].

* Corresponding author. Tel.: +91 9307025126; fax: +91 542 2368428.
E-mail addresses: maquraishi.apc@itbhu.ac.in, maquraishi@rediffmail.com (M.A. Quraishi).
Peer review under responsibility of Taibah University.

Production and hosting by Elsevier

http://dx.doi.org/10.1016/j.jtusci.2015.10.005

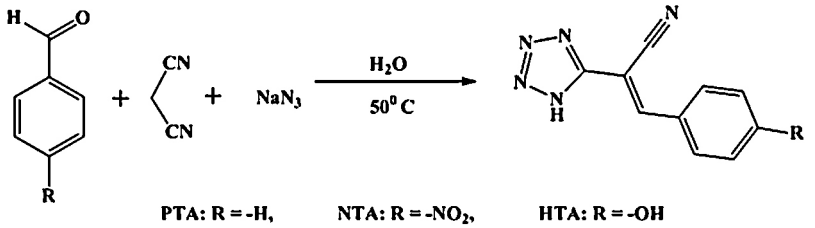

Fig. 1. Synthetic route of studied tetrazoles.

The present study is concerned with the corrosion inhibition of mild steel in 1 M HCl by three tetrazole derivatives, namely, (*E*)-3-phenyl-2-(1H-tetrazole-5-yl)acrylonitrile (PTA), (*E*)-3-(4-nitrophenyl)-2-(1H-tetrazole-5-yl)acrylonitrile (NTA), and (*E*)-3-(4-hydroxyphenyl)-2-(1H-tetrazole-5-yl)acrylonitrile (HTA), using weight loss, potentiodynamic polarization, electrochemical impedance spectroscopy (EIS), scanning electron microscopy (SEM), energy-dispersive X-ray spectroscopy (EDX), atomic force microscopy (AFM) and quantum chemical calculation methods. The selection of these compounds as corrosion inhibitors is based on the consideration that tetrazole derivatives (a) can be easily synthesized from cheap, commercially available materials, (b) exhibit high inhibition efficiency even at very low concentrations, (c) are highly soluble in the test medium, and (d) contain several heteroatoms in addition to polar functional groups (such as –CN, –OH, and $-NO_2$), multiple bonds (double bonds) and extensive conjugation in the form of aromatic rings through which they can adsorb on metal surfaces. A literature survey reveals that few systematic works have been reported on the corrosion inhibition property of tetrazole derivatives [7–12]. Quantum chemical calculations based on density functional theory (DFT) have been sufficiently developed as a powerful technique to study the interaction between inhibitors and metal surfaces [13]. The application of DFT-based calculations in the present case is constructed on the point that several theoretical parameters can be derived for even a complex molecule at very low cost [14]. Some common theoretical parameters, namely, E_{HOMO}, E_{LUMO}, ΔE, dipole moment (μ), global hardness (ρ) and global softness (σ), were derived and discussed.

2. Experimental

2.1. Materials and sample preparation

The weight loss and electrochemical experiments were performed on mild steel specimens having a chemical composition (wt.%) 0.076 wt.% C, 0.192 wt.% Mn, 0.012 wt.% P, 0.026 wt.% Si, 0.050 wt.% Cr, 0.023 wt.% Al, and the balance Fe. The exposed dimensions were 2.5 cm × 2.0 cm × 0.025 cm and 1 cm^2 for the weight loss and electrochemical experiments, respectively. Before exposure to the test solution, the exposed areas were cleaned with SiC emery papers with different grades (600–1200 mesh size), washed with deionized water, degreased with acetone and finally dried and stored in moisture-free desiccators. The test solution of 1 M HCl was prepared by diluting analytical grade HCl (MERCK, 37%) in double deionized water.

2.2. Synthesis of inhibitors

The tetrazoles used in the present study were synthesized according to a previously described procedure [15], as shown in Fig. 1. The completion of the reaction was verified by the disappearance of the starting materials on TLC plates. The characterization data, IUPAC names, structures and abbreviations used for the synthesized tetrazoles are given in Table 1.

2.3. Weight loss measurements

The weight loss experiments were performed by immersing the mild steel specimens in 100 ml of test solution without and with different concentrations of the tetrazoles. After 3 h immersion time, the mild steel specimens were taken out, cleaned with distilled water, dried and accurately weighed. Each experiment was performed in triplicate to ensure reproducibility, and the mean value was reported. The inhibition efficiency (η%) was calculated using the relation

$$\eta\% = \frac{w_0 - w_i}{w_0} \times 100 \quad (1)$$

where w_0 and w_i are the weight loss (in mg) in the absence and presence of the tetrazoles, respectively. From the calculated η%, the surface coverage (θ) was derived using the equation

$$\theta = \frac{\eta\%}{100} \quad (2)$$

Table 1
IUPAC name, molecular structure, molecular formula, melting point and analytical data of studied tetrazoles.

S. no.	IUPAC name	Chemical structure	Analytical data
1	(*E*)-3-Phenyl-2-(1H-tetrazole-5-yl)acrylonitrile (PTA)	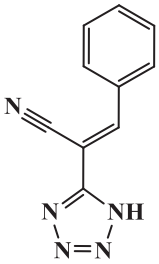	Cream color powder, mol. wt. $C_{10}H_7N_5$: MP 167–170 °C, IR (KBr, 1 cm^{-1}): 3596, 2278, 2142, 1626, 1614, 1428, 1386, ^{1}H NMR (300 MHz, DMSO, δ, ppm): 3.89, 4.24, 7.63, 8.27, 8.53
2	(*E*)-3-(4-Nitrophenyl)-2-(1H-tetrazole-5-yl)acrylonitrile (NTA)	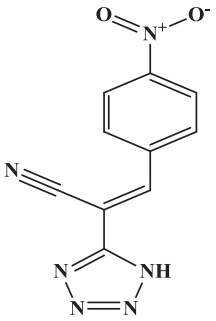	Cream color powder, mol. wt. $C_{10}H_6N_6O_2$: MP 166–168 °C, IR (KBr, 1 cm^{-1}): 3354, 3318, 2253, 1608, 1573, 1436, ^{1}H NMR (300 MHz, DMSO, δ, ppm): 3.42, 4.71, 8.18, 8.36, 8.48
3	(*E*)-3-(4-Hydroxyphenyl)-2-(1H-tetrazole-5-yl)acrylonitrile (HTA)	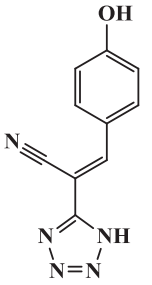	White color powder, mol. wt. $C_{10}H_7N_5O$: MP 158–161 °C, IR (KBr, 1 cm^{-1}): 3563, 3323, 2238, 1603, 1577, 1509, 1412, ^{1}H NMR (300 MHz, DMSO, δ, ppm): 5.45, 6.89, 7.28, 8.28, 9.46

2.4. Electrochemical measurements

A conventional three-electrode cell consisting of a mild steel specimen having a working area of 1 cm^2 as a working electrode, a platinum mesh as a counter electrode and saturated calomel as a reference electrode was used for all electrochemical measurements. Before each measurement, the specimens were allowed to corrode freely, and their OCPs (open circuit potentials) were measured as a function of time to obtain the steady-state potential. The anodic and cathodic Tafel curves were recorded by applying a current of ±0.25 mV with respect to the OCP at a sweep rate of 1.0 mV s^{-1}. The EIS study was carried out under potentiodynamic conditions using an AC signal of a 10 mV amplitude sinusoidal current, after the stabilization of the OCP in the frequency range of 100 kHz–0.01 Hz.

2.5. Surface measurements

The surface morphological study of the working electrode after 3 h immersion time with and without tetrazoles at a 5 kV accelerating voltage was performed using an SEM model Zeiss Evo 50 XVP instrument at 500× magnification. The change in the elements present at the surface of the working electrode was determined by an EDX detector coupled with SEM. Atomic force microscopy (AFM) was performed with and without tetrazoles using an NT-MDT multimode AFM (Russia)

Table 2
The weight loss parameters obtained for mild steel in 1 M HCl containing different concentrations of tetrazoles.

Inhibitor	Conc ($mg\,L^{-1}$)	C_R ($mg\,cm^{-2}\,h^{-1}$)	Surface coverage (θ)	$\eta\%$
Blank	0.0	7.66	–	–
PTA	10	1.96	0.7441	74.41
	20	1.00	0.8695	86.95
	30	0.66	0.9138	91.38
	40	0.46	0.9399	93.99
NTA	10	1.90	0.7519	75.19
	20	0.86	0.8877	88.77
	30	0.43	0.9438	94.38
	40	0.26	0.9660	96.60
HTA	10	1.46	0.8093	80.93
	20	0.53	0.9308	93.08
	30	0.20	0.9738	97.38
	40	0.10	0.9869	98.69

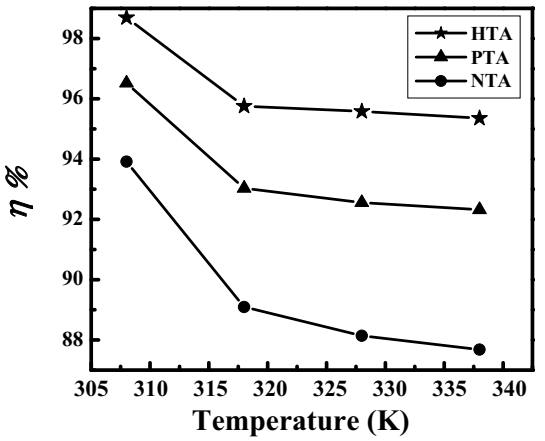

Fig. 2. Variation of inhibition efficiency with temperature.

controlled by a Solver scanning probe microscope controller.

2.6. Quantum chemical measurements

Quantum chemical calculations were carried out using the standard Gaussian 03, E.01 software package [16]. The molecular optimization of the studied tetrazoles was achieved using the functional hydride B3LYP density functional theory (DFT) formalism, having an electron basis set 6-31G (d, p) for all atoms. The quantum chemical parameters were calculated for molecules in the neutral as well as protonated form for comparison. It is well known that the phenomenon of electrochemical corrosion occurs in the liquid phase. Quantum chemical parameters such as the E_{LUMO} (energy of the highest occupied molecular orbital), E_{HOMO} (energy of the lowest unoccupied molecular orbital), $\Delta E = E_{HOMO} - E_{LUMO}$ (energy band gap), dipole moment (μ), global softness (σ), and global hardness (ρ) were measured and discussed.

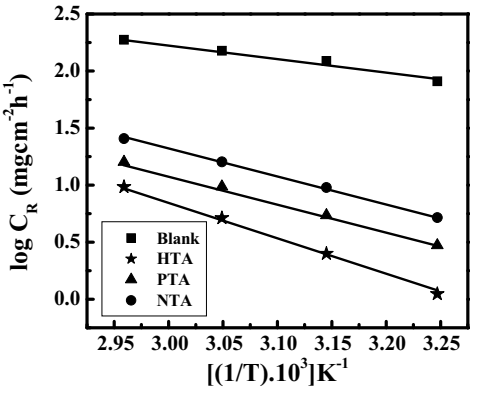

Fig. 3. Arrhenius plot of log C_R versus $1000/T$ for mild steel corrosion in 1 M HCl.

Table 3
Values of activation energies for mild steel dissolution in 1 M HCl in the absence and at optimum concentration of tetrazoles.

Inhibitor	E_a ($kJ\,mol^{-1}$)
Blank	28.48
PTA	62.40
NTA	48.75
HTA	45.95

3. Results and discussion

3.1. Weight loss experiments

3.1.1. Effect of tetrazole concentration

Table 2 presents the variation of the corrosion rate (C_R) and percentage inhibition efficiency ($\eta\%$) obtained in the weight loss experiments at different tetrazole concentrations in 1 M HCl at 308 K. The results show that the $\eta\%$ increases upon increasing the tetrazole concentrations, and maximum values of $\eta\%$ for all studied tetrazoles were obtained at 40 $mg\,L^{-1}$. A further increase in concentration did not cause any significant change in the inhibition performance. The $\eta\%$ of the three studied tetrazoles follows the order HTA (98.69%) > PTA (96.52%) > NTA (93.91%).

3.1.2. Effect of temperature

The weight loss experiments were also performed at different temperatures (308–338 K) in the absence and presence of tetrazoles at 40 $mg\,L^{-1}$ concentration for 3 h immersion time. Fig. 2 presents the variation of the $\eta\%$

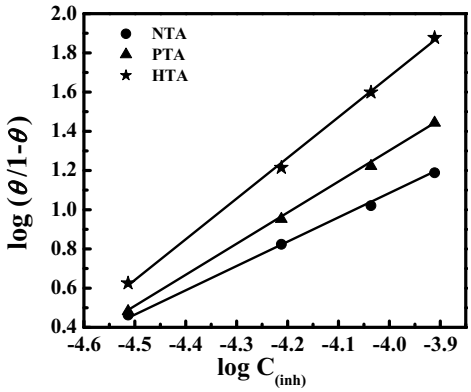

Fig. 4. Langmuir isotherm plots for the adsorption of tetrazoles on mild steel surface in 1 M HCl.

Table 4
The values of K_{ads} and ΔG^0_{ads} for mild steel in absence and presence of optimum concentration of tetrazoles in 1 M HCl at different studied temperature.

Inhibitor	K_{ads} (10^4 M^{-1})				$-\Delta G^0_{ads}$ (kJ mol^{-1})			
	308	318	328	338	308	318	328	338
PTA	1.85	0.98	0.87	0.85	34.92	35.45	35.76	36.73
NTA	3.32	1.60	1.49	1.44	36.22	36.96	37.17	38.21
HTA	9.04	3.47	1.23	0.56	37.61	38.68	39.52	39.71

with the solution temperature. It is observed that $\eta\%$ decreases upon increasing the temperature. Moreover, from Fig. 2, it is observed that the decrease in $\eta\%$ upon increasing the solution temperature is more pronounced in the lower temperature range, whereas in the high temperature range, a very slight change was observed. This decrease in $\eta\%$ at elevated temperatures might be due to the desorption of adsorbed tetrazole molecules, leading to a larger exposure of the metal to the acid solution. Moreover, the decrease in the inhibition performance upon increasing the solution temperature indicates the physical adsorption [17]. The value of the apparent activation energy (E_a) provides mechanistic information about the adsorption of the inhibitor on the metal surface. The value of E_a in the present case was calculated by applying the Arrhenius equation,

$$C_R = A \exp\left(\frac{-E_a}{RT}\right) \quad (3)$$

where C_R is the corrosion rate, R the gas constant, T the absolute temperature, and A the pre-exponential factor. A plot of log C_R vs. 1000/T for the inhibited and uninhibited mild steel specimens is shown in Fig. 3, from the slope of which values of E_a were calculated, as given in Table 3. Inspection of the tabulated data reveals that the values of E_a for the inhibited

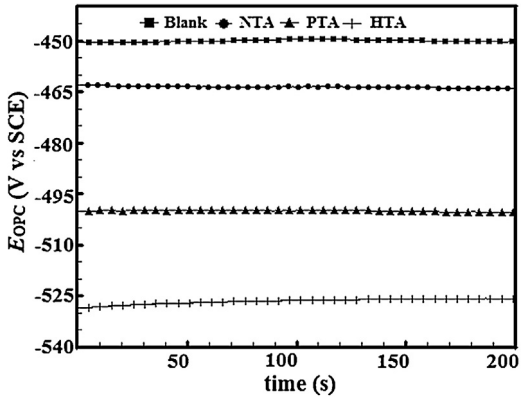

Fig. 5. OCP curves for mild steel in 1 M HCl without and with 40 mg L^{-1} concentrations of tetrazoles.

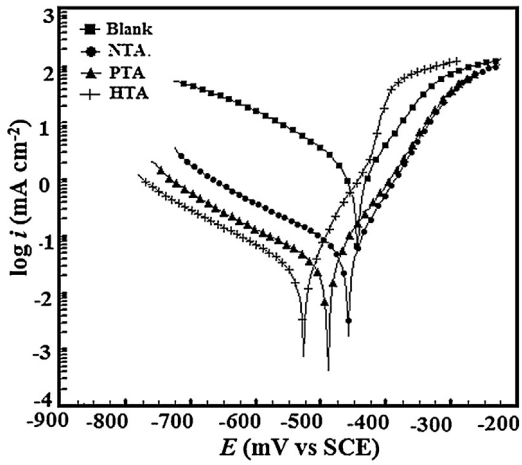

Fig. 6. Polarization curves for mild steel in the absence and presence of the optimum concentration of tetrazoles.

solution are always higher than those of the uninhibited solution, suggesting the retardation of the corrosion process through the formation of a protective surface metal-inhibitor complex [18,19]. The higher values of E_a in the presence of tetrazoles suggest that tetrazoles inhibit mild steel corrosion by forming an energy barrier to the corrosion process [19].

3.1.3. Adsorption isotherms

Because the adsorption isotherm provides some structural and thermodynamic information, it is of great importance in the corrosion field [20]. Generally, the adsorption of synthetic inhibitors is largely influenced by the nature of the testing media, the chemical structure and nature of substituents, the charge distribution, and the nature of the metal [21]. To find a suitable adsorption isotherm in the present study, several commonly used isotherms were tested, among which the Langmuir

Table 5
Tafel polarization parameters for mild steel in 1 M HCl in absence and presence of tetrazoles at 40 mg L^{-1} concentration.

Inhibitor	E_{corr} (mV/SCE)	i_{corr} ($\mu A/cm^2$)	β_a (mV/dec)	β_c (mV/dec)	θ	$\eta\%$
Blank	−445	1150	70.5	114.6	–	–
NTA	−459	61.3	58.4	177.3	0.9466	94.66
PTA	−490	40.3	68.1	266.2	0.9649	96.49
HTA	−528	26.0	52.4	165.6	0.9773	97.73

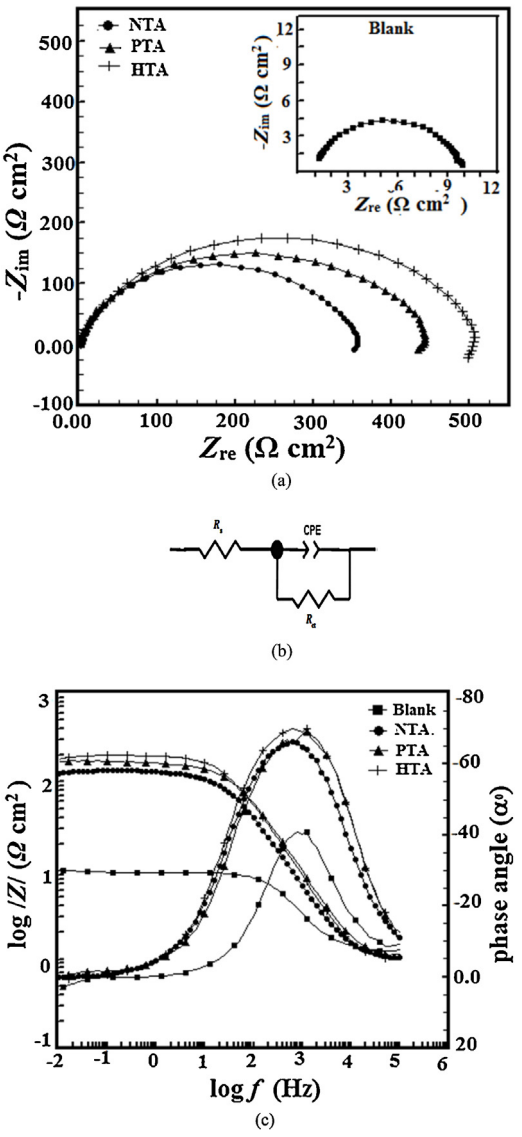

Fig. 7. (a) Nyquist plot for mild steel in 1 M HCl without and with optimum concentrations of tetrazoles. (b) Equivalent circuit model used to fit the EIS data. (c) Bode ($\log f$ vs $\log |Z|$) and phase angle ($\log f$ vs. α^0) plots for mild steel in 1 M HCl in the absence and presence of the optimum concentration of tetrazoles.

adsorption isotherm was found to fit well with our experimental data. The Langmuir isotherm can be represented as

$$\frac{C_{(inh)}}{\theta} = \frac{1}{K_{(ads)}} + C_{(inh)} \quad (4)$$

where $C_{(inh)}$ is the inhibitor concentration, K_{ads} is the equilibrium constant for the adsorption–desorption process and θ is the surface coverage. The values of K_{ads} were calculated with the help of the Langmuir plot shown in Fig. 4. The K_{ads} is related to the standard free energy (ΔG^0_{ads}) of adsorption by the relation [22]

$$\Delta G^0_{ads} = -RT \ln(55.5 K_{ads}) \quad (5)$$

where R is the universal gas constant, T is the absolute temperature in K, and the numerical value 55.5 represents the molar concentration of water in the acid solution. The calculated values of K_{ads} and ΔG^0_{ads} at the different studied temperatures are listed in Table 4. Generally, a high value of K_{ads} is associated with high adsorption efficiency. In our present case, the values of K_{ads} follow the order NTA < PTA < HTA, which is consistent with the order of the inhibition efficiency. The negative values of ΔG^0_{ads} (Table 4) suggest that the tetrazoles are spontaneously adsorbed on the mild steel surface [23]. Generally, a value of ΔG^0_{ads} of $-20\,kJ\,mol^{-1}$ or less negative is associated with physical adsorption resulting from electrostatic interaction between a charged inhibitor and charged metal, and a value of ΔG^0_{ads} of $-40\,kJ\,mol^{-1}$ or more negative is associated with chemical adsorption resulting from charged (electron) sharing between non-bonding π-electrons of the inhibitor and the d-orbitals of the surface Fe-atoms [24]. In our present study, the values of ΔG^0_{ads} were found to be between −34.92 and $-39.71\,kJ\,mol^{-1}$, suggesting that the investigated tetrazoles are adsorbed on the mild steel surface by a physiochemisorption mechanism [25]. Further, careful examination of the results shows that the values of ΔG^0_{ads} are closer to $-40\,kJ\,mol^{-1}$, suggesting that although the tetrazoles are adsorbed by a physiochemisorption

Table 6
EIS parameters obtained for mild steel in 1 M HCl in absence and presence of tetrazoles at 40 mg L^{-1} concentration.

Inhibitor	R_s ($\Omega\,cm^2$)	R_{ct} ($\Omega\,cm^2$)	C_{dl} ($\mu F\,cm^{-2}$)	n	θ	$\eta\%$
Blank	1.12	9.58	106.21	0.827	–	–
NTA	1.005	345.59	28.09	0.840	0.9722	97.22
PTA	0.858	420.54	27.90	0.856	0.9722	97.72
HTA	0.999	486.60	18.06	0.859	0.9803	98.03

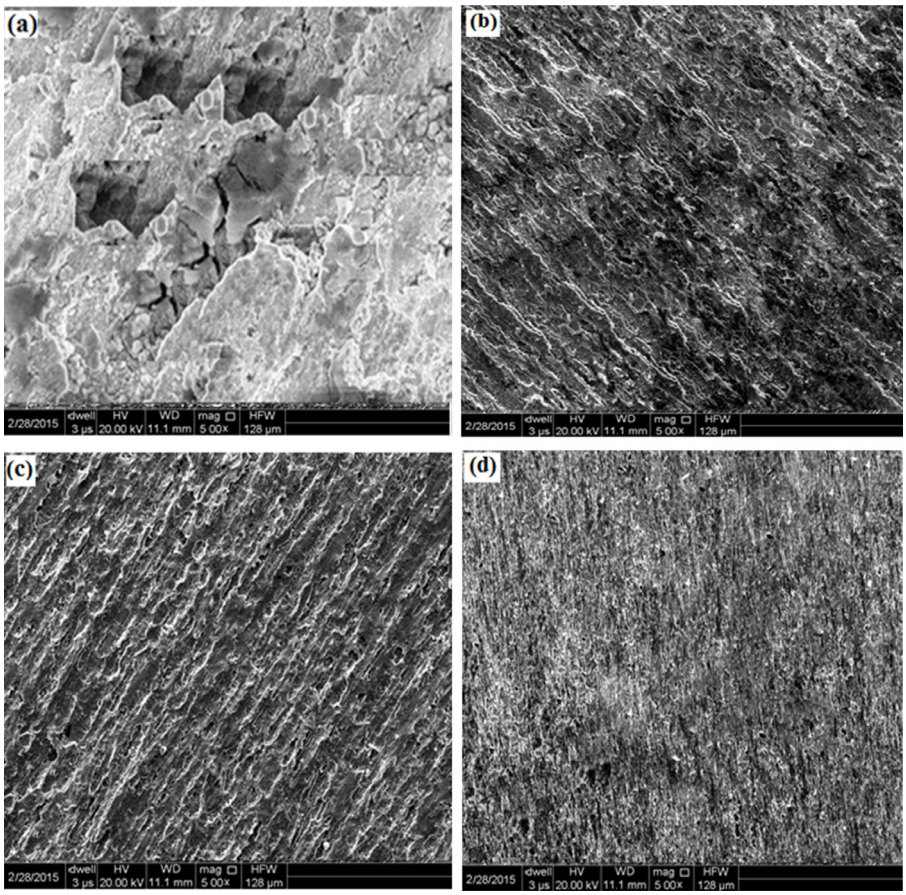

Fig. 8. SEM images of mild steel: (a) in the absence of tetrazoles and in the presence of 40 mg L^{-1} of (b) NTA, (c) PTA, and (d) HTA.

mechanism, they are predominantly adsorbed by a chemisorption mechanism [26].

3.2. Electrochemical measurements

3.2.1. Open circuit potential (OCP) curves

The potential developed on the mild steel (working) electrode relative to the potential of the reference (saturated calomel) electrode is termed the open circuit potential (OCP). The stabilization of the OCP is essential before performing the electrochemical measurements. The variation of the OCP of the working electrode with respect to time (for 200 s) in the 1 M HCl in absence and presence of 40 mg L^{-1} concentrations of the studied tetrazoles is shown in Fig. 5. The OCP curves were recorded after allowing the working electrode to corrode freely for 30 min, which is essential for the stabilization of the steady-state potential. The OCP curves give a straight line in the absence and presence of tetrazoles, suggesting that the steady-state potential has been established after 30 min immersion. It can be observed from the OCP curves that in the presence of tetrazoles, the steady-state potential (E_{corr}) shifts toward the more negative direction without changing the common features of

the OCP vs. time curves. This suggests that the tetrazoles catalyze the oxide film dissolution [27].

3.2.2. Potentiodynamic polarization studies

The potentiodynamic polarization study was performed in the absence and presence of the optimum concentrations of the studied tetrazoles. The cathodic and anodic polarization curves of mild steel in 1 M HCl are shown in Fig. 6, and the corresponding polarization parameters, including the corrosion potential (E_{corr}), corrosion current density (i_{corr}) and Tafel slopes (β_a and β_c), were derived from the extrapolation of the linear segments of the cathodic and anodic Tafel curves and are given in Table 5. From the evaluated i_{corr} values, $\eta\%$ was calculated using the relation [28]

$$\eta\% = \frac{i^0_{corr} - i^i_{corr}}{i^0_{corr}} \times 100 \quad (6)$$

where i^0_{corr} and i^i_{corr} are the corrosion current densities in the absence and presence of tetrazoles, respectively. An inspection of Fig. 6 and Table 5 suggests that the presence of tetrazoles causes a remarkable decrease in the i_{corr} values by shifting both the anodic and cathodic Tafel slopes toward low current. Furthermore, it is observable that the shapes of the polarization curves are similar in the absence and presence of tetrazoles, suggesting that the tetrazoles inhibit mild steel corrosion by simply adsorbing on the mild steel surface without changing the mechanism of mild steel dissolution [29]. An inhibitor can be categorized as anodic, cathodic and/or mixed type depending upon the displacement in the values of E_{corr}. If the displacement in the E_{corr} value for the inhibited and uninhibited solutions exceeds 85 mV, then the inhibitor can be classified as a particular (cathodic or anodic) type. However, if the displacement in the E_{corr} values is less than 85 mV, then the inhibitor can be classified as mixed type. In our present case, the maximum displacements in the E_{corr} values were 14 mV (NTA), 45 mV (PTA) and 83 mV (HTA), suggesting that all the studied tetrazoles behave as mixed type [30]. Moreover, an examination of the results shows that the cathodic reactions are more affected than the anodic reactions, suggesting that although the tetrazoles act as mixed type inhibitors, they have a pronounced effect on cathodic reactions (predominantly cathodic type) [31,32].

3.2.3. Electrochemical impedance studies

Nyquist plots in the absence and presence of the optimum (40 mg L^{-1}) concentration of the studied tetrazoles in 1 M HCl are shown in Fig. 7a. It is observed that the Nyquist spectra with and without tetrazoles show a large capacitive loop in the high-frequency region, which is a characteristic feature of the metal-corroding system in acid solution. The large capacitive loop in the high-frequency region is attributed to the charge transfer processes and to the formation of the protective surface covering by the tetrazoles [33]. Moreover, the shapes of the impedance spectra are similar in the absence and presence of tetrazoles, suggesting that tetrazoles inhibit corrosion by adsorbing onto the mild steel surface without affecting the common mechanism of metal dissolution [34]. To find suitable EIS parameters, the Randle's equivalent circuit shown in Fig. 7b was used, consisting of a solution resistance (R_s) a charge transfer resistance (R_{ct}) and a constant phase element (CPE). The EIS parameters such as R_s, R_{ct}, C_{dl}, n, and $\eta\%$ were calculated using the above-mentioned equivalent circuit and are given in Table 6. $\eta\%$ was calculated with the help of R_{ct} using the relation [28]

$$\eta\% = \frac{R^i_{ct} - R^0_{ct}}{R^i_{ct}} \times 100 \quad (7)$$

where R^0_{ct} and R^i_{ct} are the charge transfer resistances without and with tetrazoles, respectively.

The value of the double-layer capacitance (C_{dl}) can be calculated by the equation:

$$C_{dl} = (Q\, R^{1-n}_{ct})^{1/n} \quad (8)$$

where Q is the CPE constant and n is the CPE exponent that is related to the surface roughness. Generally, the low value of n is associated with high surface imperfection due to the presence of surface chloride ions and corrosion products, as well as of structural and interfacial origin [34]. In our present measurements, the value of n was 0.827 for the uninhibited specimen, while for the inhibited specimens, the values were 0.840 (NTA), 0.856 (PTA) and 0.859 (HTA). The increased values of n in the presence of the different tetrazoles suggest that the surface imperfection decreases due to the formation of a protective surface film [35,36]. It is clear from the results depicted in Table 6 that the value of R_{ct} increases whereas the value of C_{dl} decreases in the presence of tetrazoles. This increase in R_{ct} and decrease in C_{dl} are attributed due to a decrease in the local dielectric constant and/or to an increase in the thickness of the electrical double layer [37,38].

The Bode modulus and phase angle plot in the absence and presence of optimum concentrations of the studied tetrazoles at their open circuit potential are shown in Fig. 7c. A careful examination of the Bode plot reveals that the value of log|Z| and the phase angle fall to zero in the high-frequency region, which is a characteristic

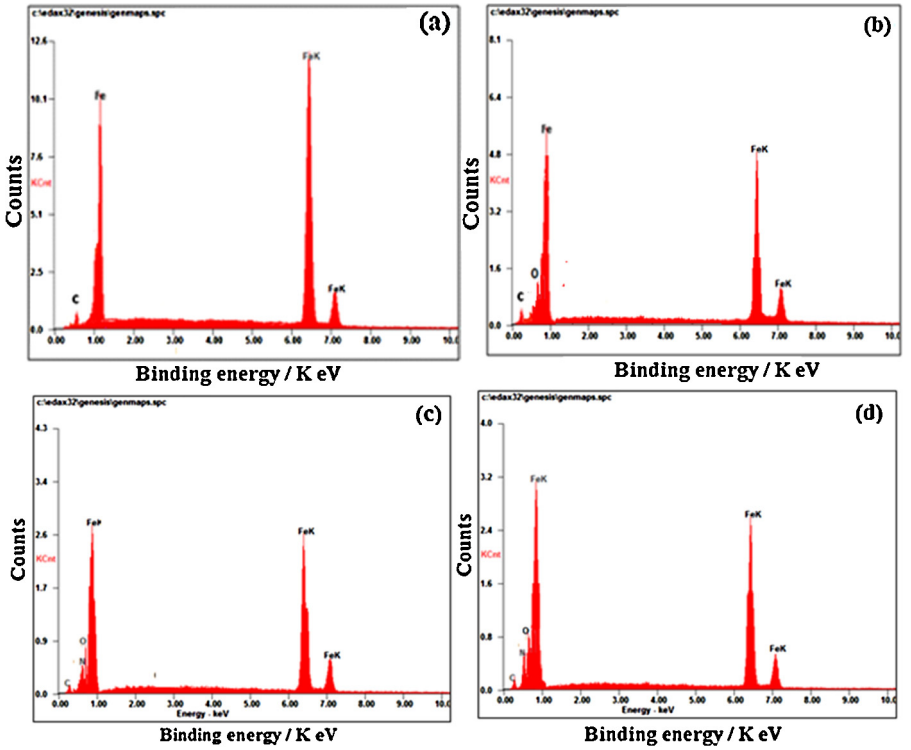

Fig. 9. EDX spectra of mild steel: (a) in the absence of tetrazoles and in the presence of 40 mg L^{-1} of (b) NTA, (c) PTA, and (d) HTA.

resistive response to the solution resistance enclosed between the working electrode and the reference electrode [39,40]. However, in the intermittent frequency region, the Bode plots give a linear relationship between $\log|Z|$ and $\log f$, with a slope near -1 and a phase angle value close to -70°, which appears to be a capacitive response of mild steel in acid solution. For an ideal capacitor, the values of the phase angle and slope should be -90° and -1, respectively. The deviation from the ideal capacitive behavior in the present case is might be due to the presence of surface imperfections [41]. The close visualization of the Bode plots further shows that the value of the phase angle remarkably increases in the presence of tetrazoles. The increased values of the phase angle in presence of tetrazoles suggest that the surface imperfection decreases due to the formation of a protective film [42].

3.3. Surface studies

3.3.1. Scanning electron microscopy (SEM) studies

To support our conclusion that the tetrazoles form protective surface films, SEM micrographs of the mild steel surface were recorded in the absence and presence of tetrazoles at 40 mg L^{-1} concentration, as shown in Fig. 8. It is seen (Fig. 8a) that in the absence of tetrazoles, the surface roughness is very high, suggesting that the mild steel surface is quite susceptible to corrosion in aggressive 1 M HCl solution. However, in the presence of tetrazoles at a 40 mg L^{-1} concentration, the surface morphologies (Fig. 8b–d) are remarkably improved. This is attributed to the formation of a protective surface film that isolates the mild steel from the aggressive acid solution.

3.3.2. Energy-dispersive X-ray spectroscopy (EDX) studies

To further support our weight loss and electrochemical finding that the tetrazoles inhibit mild steel corrosion by forming a protective film on the surface, we recorded the EDX spectra in the absence and presence of tetrazoles at 40 mg L^{-1} concentration and determined the elemental composition using energy-dispersive X-ray spectroscopy (EDX). The EDX spectra so obtained are shown in Fig. 9, and the elemental composition is given in Table 7. The EDX spectrum in the absence of tetrazoles shows characteristic signals for only iron and carbon. However, in the presence of the different studied tetrazoles (Fig. 9b–d) the EDX spectra show some additional signals corresponding to nitrogen, and

Table 7
Percentage atomic contents of elements obtained from EDX spectra of tetrazoles.

	Fe	C	N	O
Blank	63.09	36.10	–	–
PTA	65.27	27.85	6.79	–
NTA	62.74	21.48	4.89	10.87
HTA	61.54	21.65	7.42	9.24

oxygen, suggesting the presence of these elements on the surface, which could be due to the absorption of studied inhibitors on the mild steel surface. A careful examination of the EDX spectra shows that the intensity of the signals corresponding to iron significantly decreased in the presence of tetrazoles due to their significant surface coverage.

3.3.3. Atomic force microscopy (AFM) studies

The AFM micrographs of the mild steel surface after 3 h immersion time in the absence and presence of the optimum concentration of the studied tetrazoles in 1 M HCl are shown in Fig. 10. Fig. 10a shows the AFM micrograph in the absence of tetrazoles, which is characterized by a very rough electrode surface due to aggressive attack by acid. In the absence of tetrazoles, the calculated average surface roughness was 392 nm. However, in the presence of different tetrazoles (Fig. 10b–d) at 40 mg L^{-1} concentration, the AFM micrographs show remarkable improvement in the surface morphology, which could be due to the adsorption and formation of a protective film by the tetrazoles on the mild steel surface. The calculated average surface roughnesses were 138, 95 and 76 nm in the presence of PTA, NTA and HTA, respectively.

3.4. Quantum chemical calculations

3.4.1. Quantum chemical calculations for neutral forms of inhibitors

In the present study, quantum chemical calculations were performed to validate the experimental findings. Some common theoretical parameters such as the energy of the highest occupied molecular orbital (E_{HOMO}), energy of the lowest unoccupied molecular orbital (E_{LUMO}), E_{HOMO}–E_{LUMO} energy gap (ΔE), dipole moment (μ, Debye), global hardness (ρ), and global softness (σ), which provide significant information about the reactivity and adsorption characteristics of the inhibitors, were derived. The calculated theoretical parameters are given in Table 8. Figs. 11 and 12 present the optimized and frontier molecular orbital pictures of the studied tetrazoles. It is well established that the value of E_{HOMO} is often related to the electron donating tendency of the inhibitor molecules into the unoccupied d-orbital of the metal, whereas the value of E_{LUMO} is often related with the electron acceptability of the inhibitor molecules from the unoccupied d-orbital of the surface Fe-atoms [43,44]. The energy gap (ΔE) is another important parameter,

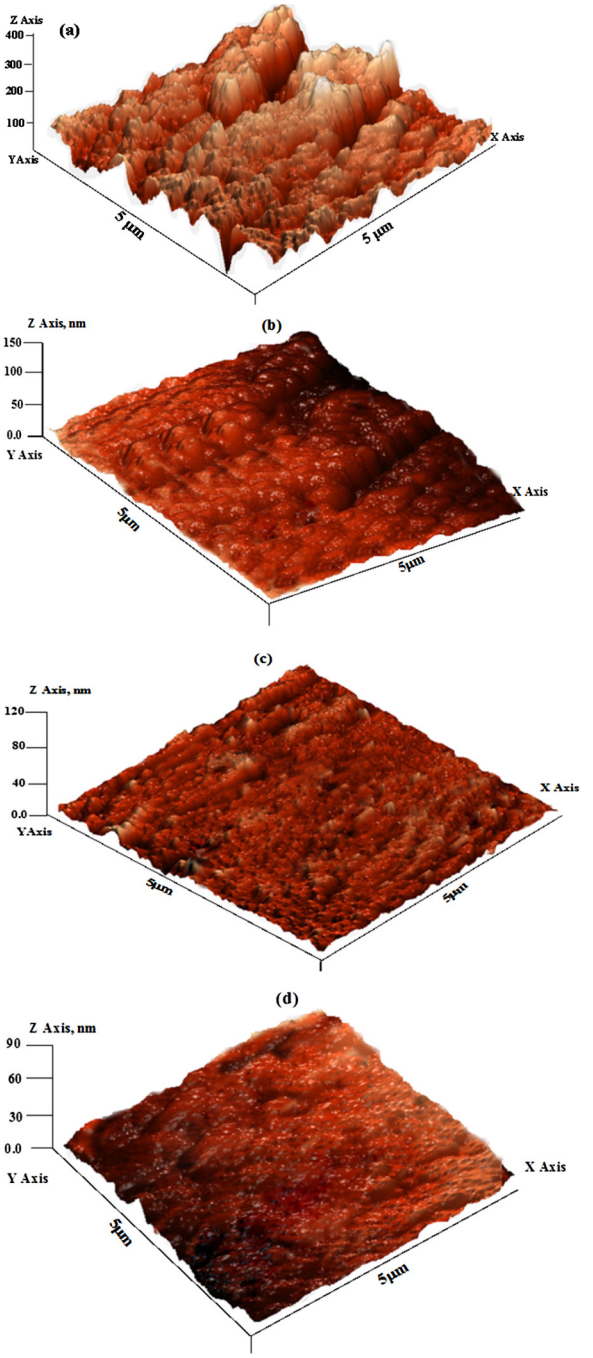

Fig. 10. AFM images of mild steel: (a) in the absence of tetrazoles and in the presence of 40 mg L^{-1} of (b) NTA, (c) PTA, and (d) HTA.

Table 8
Quantum chemical parameters for different tetrazoles calculated in gas phase.

Inhibitor	Dipole movement (μ)	E_{HOMO} (Hartree)	E_{LUMO} (Hartree)	ΔE (Hartree)	Hardness (ρ)	Softness (σ)
NTA	3.0774	−0.11721	−0.09592	0.11125	0.055625	17.9775
PTA	3.6365	−0.14874	−0.09913	0.08996	0.04498	22.2321
HTA	8.7744	−0.17760	−0.13725	0.04035	0.020175	49.5662

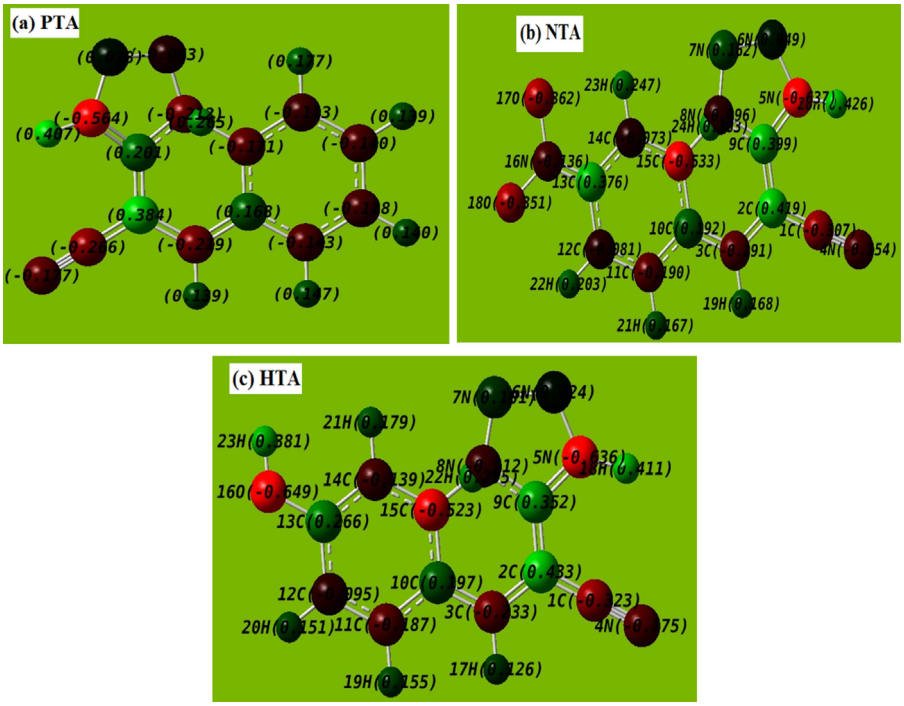

Fig. 11. Optimized structure of studied tetrazoles.

providing a measure of the chemical reactivity and complexation on the metal surfaces [45]. Generally, a low value of ΔE is associated with high chemical reactivity and therefore high inhibition efficiency [46,47]. In the present measurements, the values of ΔE follow the order HTA < PTA < NTA, which is the reverse of the order of inhibition efficiency. The decrease in the energy gap (ΔE) is consistent with the corresponding increase in global softness (σ) and decrease in global hardness (ρ). Generally, the hardness and softness are related to the molecular stability and reactivity. A soft molecule has a smaller energy gap between the E_{HOMO} and E_{LUMO}, related to higher chemical reactivity and inhibition efficiency, whereas a hard molecule has a larger energy gap between the E_{HOMO} and E_{LUMO}, related to lower chemical reactivity and inhibition efficiency [48]. Generally, the inhibition efficiency increases upon increasing the dipole moment (μ) [13]. The larger dipole moment values (Table 8) of the tetrazoles with respect to the dipole moment of water (1.88 Debye) suggest that they have a stronger dipole–dipole interaction with the mild steel surface compared to water [48]. The increase in the dipole moment increases the extension polarization, resulting in an increase in the molecular volume and thereby an increase in the inhibition efficiency [36].

3.4.2. *Quantum chemical calculations for the protonated form of the inhibitors*

Due to the presence of several nitrogen atoms, the tetrazoles considered in the present study have a strong tendency to be protonated in acidic solution. The frontier molecular orbital pictures of the protonated studied tetrazoles are shown in Fig. 13, and calculated parameters such as the energy of the highest occupied molecular orbital (E_{HOMO}), energy of the lowest unoccupied molecular orbital (E_{LUMO}), E_{HOMO}–E_{LUMO} energy gap (ΔE), dipole moments (μ, Debye), global hardness (ρ),

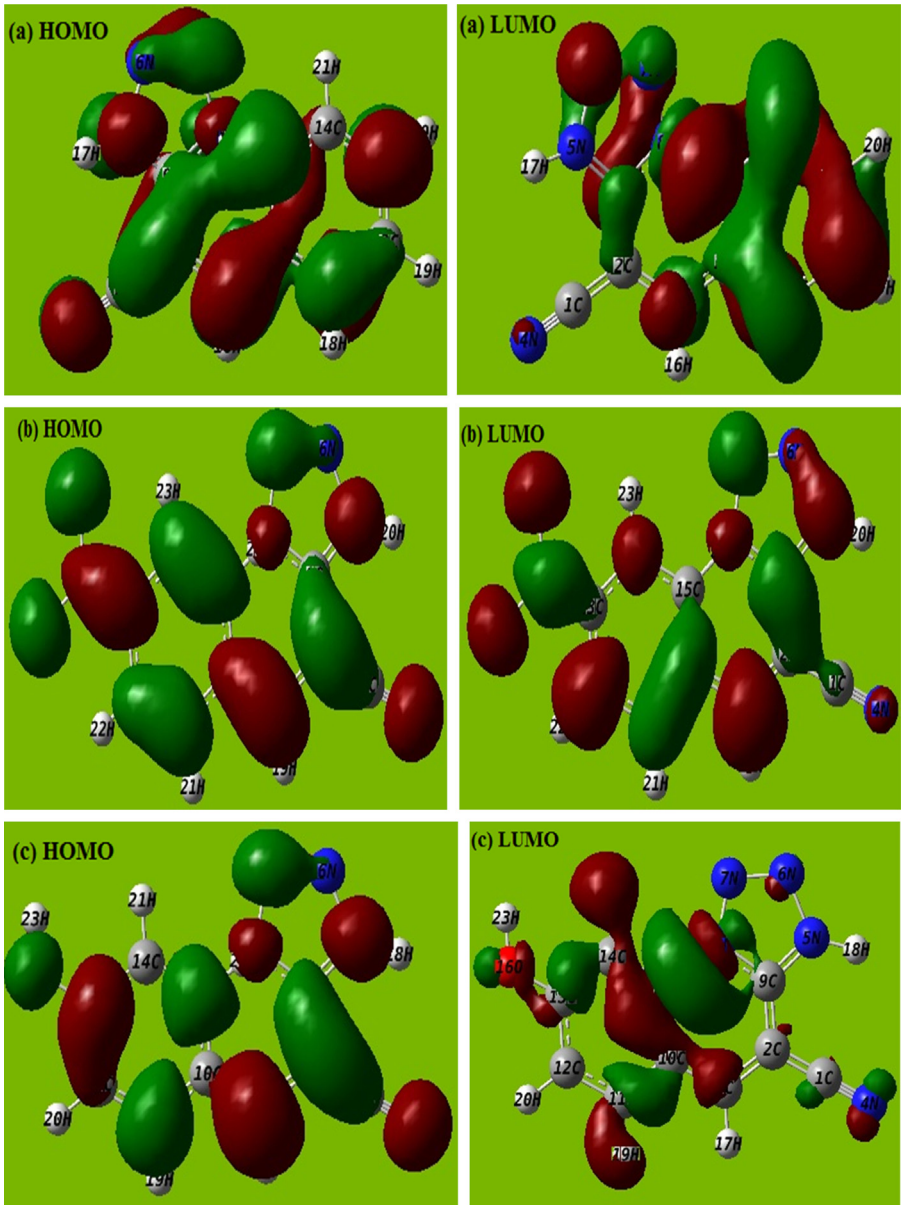

Fig. 12. Frontier molecular orbital of studied tetrazoles: (a) NTA (left, HOMO; right, LUMO), (b) PTA (left, HOMO; right, LUMO) and (c) HTA (left, HOMO; right, LUMO).

and global softness (σ) are given in Table 9. It may be observed that most of the quantum chemical parameters for the protonated forms of the tetrazoles are in accordance with the quantum chemical parameters obtained for the neutral forms. The dipole moment follows the order HTA > PTA > NTA, which is in accordance with the order of inhibition efficiency. The inhibition efficiency also increases with the decreasing energy gap (ΔE) between E_{HOMO} and E_{LUMO}. Obviously, the values of global softness (σ) and inhibition follow the order HTA > PTA > NTA.

4. Mechanism of inhibition

Fig. 14 shows the skeleton representation of the adsorption of the tetrazole molecules on the mild steel surface. Generally, the adsorption of the inhibitor on the metal surface is a complex phenomenon that can be considered as physiochemisorption (mixed adsorption) rather than purely physical or chemical adsorption [49]. The physical adsorption occurs via electrostatic interaction between the oppositely charged inhibitor molecule and metal surface, whereas chemical adsorption takes

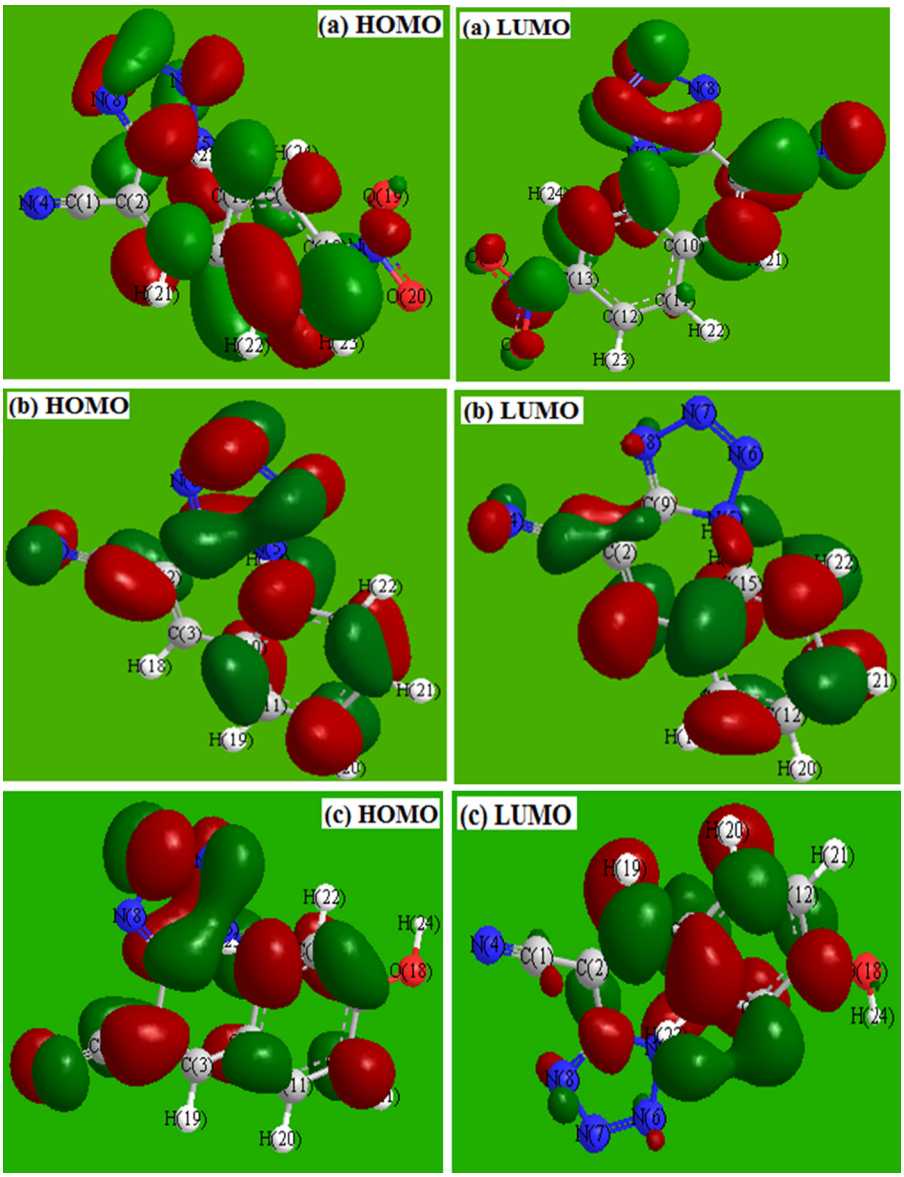

Fig. 13. Frontier molecular orbital for protonated forms of studied tetrazoles: (a) NTA (left, HOMO; right, LUMO), (b) PTA (left, HOMO; right, LUMO) and (c) HTA (left, HOMO; right, LUMO).

place via donor–acceptor interactions between unshared electron pairs of heteroatoms (such as N, O), π-electrons of the multiple bonds of aromatic rings and polar functional groups with the empty d-orbital of the surface iron atoms [50]. The heteroatoms present in the inhibitor molecule get protonated in aqueous acidic solution due to the presence of unshared electron pairs on them. It is well known that the mild steel surface is positively charged

Table 9
Quantum chemical parameters for different protonated tetrazoles calculated in aqueous phase.

Inhibitor	Dipole movement (μ)	E_{HOMO} (Hartree)	E_{LUMO} (Hartree)	ΔE (Hartree)	Hardness (ρ)	Softness (σ)
NTA	1.6270	−0.10319	−0.040056	0.06313	0.03156	31.6856
PTA	3.2903	−0.07801	−0.11895	−0.04094	−0.02047	48.8511
HTA	8.627	−0.08334	−0.09962	−0.01628	−0.00814	122.8501

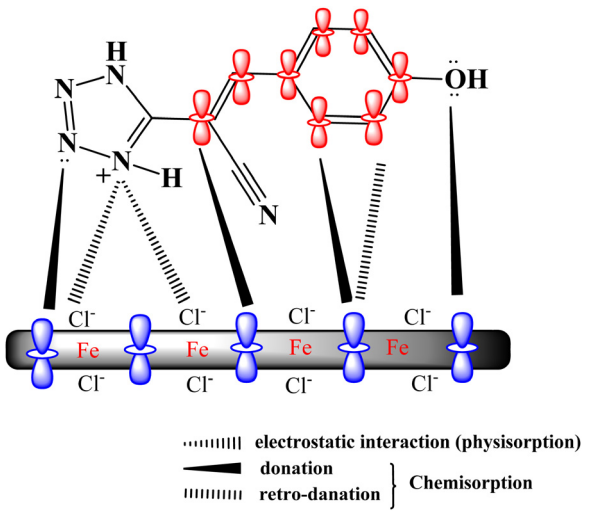

Fig. 14. Pictorial representation of the adsorption behavior of the tetrazoles on mild steel in 1 M HCl solution.

with respect to the potential of zero charge (PZC) in hydrochloric acid solutions [51]. Because the chloride ions have a small degree of hydration, they preferably adsorb on the positively charged metal surface [52]. The positively charged inhibitor molecule attracts the negatively charged mild steel (due to adsorption of chloride ions) via electrostatic interaction (physisorption). However, due to loss of H_2 gas on the cathode, the cationic form of the inhibitor reverts to its neutral form, and the heteroatoms with free unshared electron pairs are adsorbed by donor–acceptor interactions (chemisorption) [53]. This suggests that physisorption is only a precursor stage of the chemisorption. In the present study, the efficiency of the studied tetrazoles follows the order HTA > PTA > NTA. The best inhibition performance of the HTA among studied tetrazoles is attributed due to the presence of the ring activator –OH group in the phenyl moiety, whereas the lowest inhibition efficiency of NTA is due to the presence of the ring deactivator $-NO_2$ group in the phenyl moiety.

5. Conclusions

The present study shows that the investigated tetrazoles are efficient corrosion inhibitors for mild steel in 1 M HCl, and their order of inhibition efficiency is HTA > PTA > NTA. Weight loss measurements show that the extent of surface coverage and inhibition efficiency increases with the tetrazole concentrations, and the maximum inhibition efficiency was obtained at 40 mg L^{-1} concentration. The adsorption of tetrazoles on the mild steel surface obeys the Langmuir adsorption isotherm. The values of the activation energy (E_a) show that tetrazoles inhibit mild steel corrosion by forming an energy barrier to the corrosion process. The values of the Gibbs free energy suggest that the tetrazoles have a strong tendency to adsorb spontaneously on the mild steel surface. Polarization studies show that tetrazoles are cathodic inhibitors. EIS measurements indicate that the thickness of the electric double layer increases due to the adsorption of tetrazoles at the metal/electrolyte interface. SEM and EDX studies indicate that the tetrazoles form a protective surface covering. A good correlation has been found between quantum chemical calculations and the results obtained experimentally.

References

[1] H.M. Abd El-Lateef, Experimental and computational investigation on the corrosion inhibition characteristics of mild steel by some novel synthesized imines in hydrochloric acid solutions, Corros. Sci. 92 (2015) 104–117.
[2] C. Verma, A. Singh, G. Pallikonda, M. Chakravarty, M.A. Quraishi, I. Bahadur, E.E. Ebenso, Aryl sulfonamidomethylphosphonates as new class of green corrosion inhibitors for mild steel in 1 M HCl: electrochemical, surface and quantum chemical investigation, J. Mol. Liq. 209 (2015) 306–319.
[3] M. Finsgar, J. Jackson, Application of corrosion inhibitors for steels in acidic media for the oil and gas industry: a review, Corros. Sci. 86 (2014) 17–41.
[4] D. Daoud, T. Douadi, H. Hamani, S. Chafaa, M. Al-Noaimi, Corrosion inhibition of mild steel by two new S-heterocyclic compounds in 1 M HCl: experimental and computational study, Corros. Sci. (2015), http://dx.doi.org/10.1016/j.corsci.2015.01.025.
[5] R. Hasanov, S. Bilge, S. Bilgiç, G. Gece, Z. Kılıç, Experimental and theoretical calculations on corrosion inhibition of steel in 1 M H_2SO_4 by crown type polyethers, Corros. Sci. 52 (2010) 984–990.
[6] I.B. Obot, D.D. Macdonald, Z.M. Gasem, Density functional theory (DFT) as a powerful tool for designing new organic corrosion inhibitors. Part 1: An overview, Corros. Sci. (2015), http://dx.doi.org/10.1016/j.corsci.2015.01.037.
[7] Y. Elkacimi, M. Achnin, Y. Aouine, M. Ebn Touhami, A. Alami, R. Touir, M. Sfaira, D. Chebabe, A. Elachqar, B. Hammouti, Inhibition of mild steel corrosion by some phenyltetrazole substituted compounds in hydrochloric acid, Port. Electrochim. Acta 30 (2012) 53–65.
[8] P. Liu, X. Fang, Y. Tang, C. Sun, C. Yao, Electrochemical and quantum chemical studies of 5-substituted tetrazoles as corrosion inhibitors for copper in aerated 0.5 M H_2SO_4 solution, Mater. Sci. Appl. 2 (2011) 1268–1278.
[9] K.F. Khaled, M.M. Al-Qahtani, The inhibitive effect of some tetrazole derivatives towards Al corrosion in acid solution: chemical, electrochemical and theoretical studies, Mater. Chem. Phys. 113 (2009) 150–158.
[10] F. Zucchi, G. Trabanelli, M. Fonsati, Tetrazole derivatives as corrosion inhibitors for copper in chloride solutions, Corros. Sci. 38 (1996) 2019–2029.
[11] M. El-Sayed, R.M. Sherif, J.D. Erasmus, Comins inhibition of copper corrosion in acidic chloride pickling solutions by 5-(3-aminophenyl)-tetrazole as a corrosion inhibitor, Corros. Sci. 50 (2008) 3439–3445.

[12] S. Kertit, B. Hammouti, Corrosion inhibition of iron in 1 M HCl by 1-phenyl-S-mercapto-1,2,3,4-tetrazole, Appl. Surf. Sci. 93 (1996) 59–66.
[13] I.B. Obot, Z.M. Gasem, Theoretical evaluation of corrosion inhibition performance of some pyrazine derivatives, Corros. Sci. 83 (2014) 359–366.
[14] S. Issaadi, T. Douadi, S. Chafaa, Adsorption and inhibitive properties of a new heterocyclic furan Schiff base on corrosion of copper in HCl 1 M: experimental and theoretical investigation, Appl. Surf. Sci. 316 (2014) 582–589.
[15] Z.N. Tisseh, M. Dabiri, M. Nobahar, H.R. Khavasi, A. Bazgir, Catalyst-free, aqueous and highly diastereoselective synthesis of new 5-substituted 1H-tetrazoles via a multi-component domino Knoevenagel condensation/1,3 dipolar cycloaddition reaction, Tetrahedron 68 (2012) 1769–1773.
[16] M.J. Frisch, G.W. Trucks, H.B. Schlegel, G.E. Scuseria, M.A. Robb, J.R. Cheeseman Jr., Gaussian 03, revision E.01, Gaussian Inc., Wallingford, CT, 2007.
[17] P. Mourya, P. Singh, A.K. Tewari, R.B. Rastogi, M.M. Singh, Relationship between structure and inhibition behavior of quinolinium salts for mild steel corrosion: experimental and theoretical approach, Corros. Sci. (2015), http://dx.doi.org/10.1016/j.corsci.2015.02.034.
[18] L.C. Murulana, M.M. Kabanda, E.E. Ebenso, Experimental and theoretical studies on the corrosion inhibition of mild steel by some sulphonamides in aqueous HCl, RSC Adv. 5 (2015) 28743–28761.
[19] C. Verma, P. Singh, I. Bahadur, E.E. Ebenso, M.A. Quraishi, Electrochemical, thermodynamic, surface and theoretical investigation of 2-aminobenzene-1,3-dicarbonitriles as green corrosion inhibitor for aluminum in 0.5 M NaOH, J. Mol. Liq. 209 (2015) 767–778.
[20] M.S. Nooshabadi, M. Behpour, F.S. Razavi, M. Hamadanian, V. Nejadshafieea, Study of N-benzylidene derivatives synthesized as corrosion inhibitors for copper in HCl solution, RSC Adv. 5 (2015) 23357–23366.
[21] A. Ehsani, M.G. Mahjani, R. Moshrefi, H. Mostaanzadeh, J.S. Shayeh, Electrochemical and DFT study on the inhibition of 316L stainless steel corrosion in acidic medium by 1-(4-nitrophenyl)-5-amino-1H-tetrazole, RSC Adv. 4 (2014) 20031–20037.
[22] C. Verma, M.A. Quraishi, A. Singh, 2-Aminobenzene-1,3-dicarbonitriles as green corrosion inhibitor for mild steel in 1 M HCl: electrochemical, thermodynamic, surface and quantum chemical investigation, J. Taiwan Inst. Chem. Eng. 49 (2015) 229–239.
[23] R. Yıldız, T. Dogan, I. Dehri, Evaluation of corrosion inhibition of mild steel in 0.1 M HCl by 4-amino-3-hydroxynaphthalene-1-sulphonic acid, Corros. Sci. 85 (2014) 215–221.
[24] L. Bai, L.-J. Feng, H.-Y. Wang, Y.-B. Lu, X.-W. Leid, F.-L. Bai, Comparison of the synergistic effect of counterions on the inhibition of mild steel corrosion in acid solution: electrochemical, gravimetric and thermodynamic studies, RSC Adv. 5 (2015) 4716–4726.
[25] D. Wang, B. Xiang, Y. Liang, S. Song, C. Liu, Corrosion control of copper in 3.5 wt.% NaCl solution by domperidone: experimental and theoretical study, Corros. Sci. 85 (2014) 77–86.
[26] S. Banerjee, A. Mishra, M.M. Singh, B. Maiti, B. Ray, P. Maiti, Highly efficient polyurethane ionomer corrosion inhibitor: the effect of chain structure, RSC Adv. 1 (2011) 199–210.
[27] D.K. Yadav, M.A. Quraishi, Electrochemical investigation of substituted pyranopyrazoles adsorption on mild steel in acid solution, Ind. Eng. Chem. Res. 51 (2012) 8194–8210.
[28] I. Dehri, M. Erbil, Organic sulphur-containing compounds as corrosion inhibitors for mild steel in acidic media: correlation between inhibition efficiency and chemical structure, Appl. Surf. Sci. 236 (2004) 155–164.
[29] H. Keles, M. Keles, I. Dehri, O. Serindag, Adsorption and inhibitive properties of aminobiphenyl and its Schiff base on mild steel corrosion in 0.5 M HCl medium, Colloids Surf. A 320 (2008) 138–145.
[30] M. Behpour, N. Mohammadi, E. Alian, Electrochemical and mass loss investigations of new Schiff base as corrosion inhibitor for mild steel, J. Iron Steel Res. Int. 21 (2014) 121–124.
[31] B. Zhang, C. He, C. Wang, P. Sun, F. Li, Y. Lin, Synergistic corrosion inhibition of environment-friendly inhibitors on the corrosion of carbon steel in soft water, Corros. Sci. 94 (2015) 6–20.
[32] H. Bhandari, V. Choudhary, S.K. Dhawan, Influence of self-doped poly(aniline-co-4-amino-3-hydroxy-naphthalene-1-sulfonic acid) on corrosion inhibition behaviour of iron in acidic medium, Synth. Met. 161 (2011) 753–762.
[33] K.S. Jacob, G. Parameswaran, Corrosion inhibition of mild steel in hydrochloric acid solution by Schiff base furoin thiosemicarbazone, Corros. Sci. 52 (2010) 224–228.
[34] M.A. Veloz, I. González, Electrochemical study of carbon steel corrosion in buffered acetic acid solutions with chlorides and H_2S, Electrochim. Acta 48 (2002) 135–144.
[35] K.M. Emran, Corrosion characterisation and passivation behavior of Fe68.6Ni28.2Mn3.2 alloy in acidic solution, Int. J. Electrochem. Sci. 9 (2014) 4217–4229.
[36] B.D. Mert, A.O. Yüce, G. Kardas, B. Yazıcı, Inhibition effect of 2-amino-4-methylpyridine on mild steel corrosion: experimental and theoretical investigation, Corros. Sci. 85 (2014) 287–295.
[37] M. Faustin, A. Maciuk, P. Salvin, C. Roos, M. Lebrini, Corrosion inhibition of C38 steel by alkaloids extract of *Geissospermum laeve* in 1 M hydrochloric acid: electrochemical and phytochemical studies, Corros. Sci. 92 (2015) 287–300.
[38] H. Lua, Y. Zhou, S. Vongehr, K. Hu, X. Meng, Electropolymerization of PANI coating in nitric acid for corrosion protection of 430 SS, Synth. Met. 161 (2011) 1368–1376.
[39] H.H. Hassan, Inhibition of mild steel corrosion in hydrochloric acid solution by triazole derivatives: Part II: time and temperature effects and thermodynamic treatments, Electrochim. Acta 53 (2007) 1722–1730.
[40] Sudheer, M.A. Quraishi, The corrosion inhibition effect of aryl pyrazolo pyridines on copper in hydrochloric acid system: computational and electrochemical studies, RSC Adv. 5 (2015) 41923–41933.
[41] C. Verma, P. Singh, M.A. Quraishi, A thermodynamical, electrochemical and surface investigation of Bis(indolyl)methanes as Green corrosion inhibitors for mild steel in 1 M hydrochloric acid solution, J. Assoc. Arab Univ. Basic Appl. Sci. (2015), http://dx.doi.org/10.1016/j.jaubas.2015.04.003.
[42] J.C. Liu, S.W. Park, S. Nagao, M. Nogi, H. Koga, J.S. Ma, G.g. Zhang, K. Suganuma, The role of Zn precipitates and Cl-anions in pitting corrosion of Sn–Zn solder alloys, Corros. Sci. 92 (2015) 263–271.
[43] M. Mihit, K. Laarej, H. Abou El Makarim, L. Bazzi, R. Salghi, B. Hammouti, Study of the inhibition of the corrosion of copper and zinc in HNO_3 solution by electrochemical technique and quantum chemical calculations, Arab. J. Chem. 3 (2010) 55–60.
[44] S.K. Saha, P. Ghosh, A. Hens, N.C. Murmu, P. Banerjee, Density functional theory and molecular dynamics simulation study on corrosion inhibition performance of mild steel by

mercapto-quinoline Schiff base corrosion inhibitor, Physica E 66 (2015) 332–341.
[45] B. Hammouti, A. Dafali, R. Touzani, M. Bouachrine, Inhibition of copper corrosion by bipyrazole compound in aerated 3% NaCl, J. Saudi Chem. Soc. 16 (2012) 413–418.
[46] F. Zhang, Y. Tang, Z. Cao, W. Jing, Z. Wu, Y. Chen, Performance and theoretical study on corrosion inhibition of 2-(4-pyridyl)-benzimidazole for mild steel in hydrochloric, Corros. Sci. 61 (2012) 1–9.
[47] M. Yadav, R.R. Sinha, S. Kumar, I. Bahadur, E.E. Ebenso, Synthesis and application of vernew acetohydrazide derivatives as a corrosion inhibition of mild steel in acidic medium: insight from electrochemical and theoretical studies, J. Mol. Liq. 208 (2015) 322–332.
[48] C. Verma, M.A. Quraishi, A. Singh, A thermodynamical, electrochemical, theoretical and surface investigation of diheteroaryl thioethers as effective corrosion inhibitors for mild steel in 1 M HCl, J. Taiwan Inst. Chem. Eng. (2015), http://dx.doi.org/10.1016/j.jtice.2015.06.020.
[49] A.K. Singh, Inhibition of mild steel corrosion in hydrochloric acid solution by 3-(4-((Z)-indolin-3-ylideneamino)phenylimino) indolin-2-one, Ind. Eng. Chem. Res. 51 (2012) 3215–3223.
[50] C. Verma, M.J. Reddy, M.A. Quraishi, Microwave assisted eco-friendly synthesis of chalcones using 2, 4-dihydroxy acetophenone and aldehydes as corrosion inhibitors for mild steel in 1 M HCl, Anal. Bioanal. Electrochem. 6 (2014) 321–340.
[51] S. Deng, X. Li, H. Fu, Acid violet 6B as a novel corrosion inhibitor for cold rolled steel in hydrochloric acid solution, Corros. Sci. 53 (2011) 760–768.
[52] I. Ahamad, R. Prasad, M.A. Quraishi, Adsorption and inhibitive properties of some new Mannich bases of Isatin derivatives on corrosion of mild steel in acidic media, Corros. Sci. 52 (2010) 1472–1481.
[53] D.K. Yadav, B. Maiti, M.A. Quraishi, Electrochemical and quantum chemical studies of 3,4-dihydropyrimidin-2(1H)-ones as corrosion inhibitors for mild steel in hydrochloric acid solution, Corros. Sci. 52 (2010) 3586–3598.